Direct Gas−Liquid Interfacial Dynamics: The Reaction between O(^{3}P) and a Liquid Hydrocarbon

Sven P. K. Köhler, Mhairi Allan, Matthew L. Costen, and Kenneth G. McKendrick*

School of Engineering and Physical Sciences, Heriot-Watt University, Edinburgh EH14 4AS, United Kingdom

Received: October 25, 2005; In Final Form: November 10, 2005

We report the first measurements of internal energy distributions of the OH produced via a direct mechanism, isolated from other components on the basis of time-of-flight, in the interfacial reaction between gas-phase O(^{3}P) atoms and the liquid hydrocarbon squalane, $C_{30}H_{62}$. O(^{3}P) atoms were generated by laser photolysis of NO_2 above the liquid. Resulting hydroxyl radicals that escape from the surface were detected by laser-induced fluorescence. Time-of-flight profiles demonstrate that the kinetic energy of the fastest OH ($v' = 1$) is lower than that of ($v' = 0$). Rotational distributions were measured at the rising edge of their appearance for both OH ($v' = 0$) and ($v' = 1$). They were found to differ substantially more than at the peak of their profiles. They were also less dependent on the bulk liquid temperature. We conclude that the new data confirm strongly that at least two mechanisms contribute to the production of OH. The higher-velocity component has translational and rotational energy distributions, observed cleanly for the first time, consistent with a direct mechanism. The close correspondence of these rotational distributions to those from the corresponding homogeneous gas-phase reaction of O(^{3}P) with smaller hydrocarbons suggests a very similar, near collinear direct abstraction. This is accompanied by a slower component with kinetic energy and rotational (but not vibrational) distributions reflecting the temperature of the liquid, consistent with a distinct trapping−desorption mechanism.

Introduction

Compared to the vast accumulation of knowledge on the dynamics of elementary chemical reactions in the pure gas phase,[1] reactions at the gas-condensed phase interface have received much less attention. Within this class, reactions on solid surfaces have been studied in significantly greater detail than gas−liquid reactions.[2] This is mainly for two reasons: one of motivation and the other of feasibility. Gas−solid reactions model important processes in heterogeneous catalysis,[2a] providing an early stimulus to their investigation. It is also easier to conduct experiments with solids rather than liquids in the high-vacuum environment needed to obtain collision-free conditions. These "nascent" conditions are crucial to experiments aimed at inferring the mechanism of a chemical reaction from the observed motions of the products.

However, despite the relative lack of knowledge of their detailed mechanisms, collisions between gas-phase atoms or molecules and liquids are also clearly important. Their relevance spans a diversity of atmospheric (e.g. mass transfer and reaction at the surface of the sea and of aerosol particles), industrial (e.g. distillation, propellant combustion), and biological (e.g. respiration) contexts. Experimental attempts to gain some insight into these phenomena do date back almost 50 years,[3] but these early studies were confined to scattering atomic and molecular gases from molten metals. The first studies of inelastic scattering from less esoteric liquids were not conducted until much more recently. Nathanson and co-workers are primarily responsible for this development, through the introduction of low-vapor-pressure polyatomic liquids such as squalane, glycerol, and perfluoropolyether.[4] Using mass spectrometric detection, it was clear that the time-of-flight profiles of the inelastically scattered species are composed of two different components. The molecules either come off the surface with a kinetic energy close to their initial energy (the "direct" component) or they are trapped at the surface for a finite time and leave the surface with a Boltzmann kinetic energy distribution (a "trapping−desorption" mechanism). A similar combination of direct and indirect inelastic scattering mechanisms was found by McCaffery and co-workers and very recently by Nesbitt and co-workers by alternative spectroscopic approaches.[5] McCaffery and co-workers[5a] used LIF to measure the internal energy distributions of inelastically scattered molecular iodine from methylated polysiloxane oil and liquid gallium surfaces. Nesbitt and co-workers[5b] directed a seeded CO_2 beam onto a liquid perfluoropolyether surface and detected the rotational and translational energy distributions of two vibrational levels by high-resolution absorption spectroscopy.

In the present work, we shall be concerned with the surface oxidation of liquid hydrocarbons. Viewed generally, these processes play an important role in a number of fields. These include the combustion of fuels and the undesired oxidation of lubricants in internal combustion engines, for example. They are also key steps in the processing of atmospheric aerosols containing even trace-levels of organic constituents. These particles are found to form a micelle-like structure, with their hydrophobic components accumulated at the outer surface of a hydrophilic core.[6] They are consequently inert to the uptake of water. Subsequent oxidation, in most regions of the atmosphere predominantly by the hydroxyl radical but in some cases also by ozone and other oxidants, creates hydrophilic sites on the external surfaces. This enables them to capture water efficiently and hence act as cloud condensation nuclei. This phenomenon has motivated kinetic experiments[7] on reactions between

* To whom correspondence should be addressed. E-mail: k.g.mckendrick@hw.ac.uk.

10.1021/jp056128q CCC: $33.50
Published on Web 01/21/2006

atmospherically relevant gas-phase oxidants and condensed-phase hydrocarbon layers. Naaman and co-workers and Moise and Rudich measured the rate constant between $O(^3P)$ and organized monolayers consisting of saturated hydrocarbon chains. They found that it exceeds the gas-phase rate constant by some 3 orders of magnitude. Similarly, the reaction of OH radicals with a number of hydrocarbon surfaces, investigated by Molina and co-workers, shows an increased reactivity over related gas-phase experiments. These observations have led to various speculations on the mechanistic reason for the enhancement.[7b]

One further specific reason for the burgeoning interest in the dynamics of the reaction between $O(^3P)$[8] or O^+[9] and hydrocarbon surfaces is their relevance to the degradation of polymer heatshields on satellites in low-Earth orbit (LEO), in the range 200−700 km.[10] $O(^3P)$ and O^+ are the most abundant neutral and ionic species at these altitudes. They collide with satellites at collision energies as high as 5 eV. This has motivated a series of experiments by Minton, initially in collaboration with Casavecchia and subsequently with a number of other co-workers.[8,11] These experiments are most closely related to the ones that we describe here in that they investigate the same system, $O(^3P)$ + squalane. They represented a major step forward because they were the first investigations of *reactive* collisions between gas-phase species and liquid surfaces to extract dynamical information on the gas-phase products. They used molecular beam scattering methods to measure angle-resolved kinetic-energy profiles over a wide range of collision energies, extending up to 5 eV (482 kJ mol^{-1}). At the upper end of this energy range additional chemical channels involving C−C bond scission become feasible. In the current work we explore only lower energies where the sole significant primary channel is abstraction of a hydrogen atom.

Minton and Casavecchia's experiments showed that inelastically scattered oxygen atoms are the main gas-phase species leaving the surface, but the reactive products OH and H_2O were also observed. The time-of-flight profiles of all three species consisted of fast and slow components, ascribed to direct and trapping−desorption mechanisms analogous to those in the inelastic scattering experiments described above.

Finally and most recently, our own previous experiments made another complementary step forward by measuring the corresponding *internal* energy distribution of the hydroxyl radicals produced by reaction of $O(^3P)$ with a squalane surface.[12] Using laser-based photolytic initiation and laser-induced fluorescence (LIF) detection, nascent OH rotational state distributions and branching ratios between the two lowest vibrational levels were measured. Results of experiments at different liquid surface temperatures led us to the conclusion, consistent with the previous molecular beam measurements of product velocities but based independently on *rotational* distributions, that the oxygen atoms react at the surface through a combination of direct and trapping−desorption mechanisms.[12b] We were also able to record relatively low-resolution time-of-flight profiles of the hydroxyl radicals, which contain independent *state-specific* information on their velocities. At one level, these are valuable simply in verifying that the observed OH radicals originate from the liquid squalane surface. Beyond that, it proved possible to simulate these profiles successfully in a Monte Carlo fashion using a combination of the velocity distributions anticipated for trapping−desorption and direct mechanisms.

Importantly, all our previous measurements were confined to the peak of the appearance profile of the recoiling OH products, where we believe that the direct and the trapping−desorption mechanisms contribute roughly equal amounts to the overall distribution. The new results we report in this paper are the first measurements of internal energy distributions of the (dynamically more interesting) direct component in isolation. We have done this by exploiting a combination of time-of-flight resolution of translational energy components and the inherently state-specific nature of LIF detection. This allows us to determine correlations between the kinetic and internal state distributions of the OH products. This novel dynamical information provides clearer insight into the mechanism of this benchmark gas−liquid interfacial reaction.

Experimental Section

Only a brief description of the experimental setup will be provided as it has been described in detail elsewhere.[12] The partially branched liquid hydrocarbon squalane (2,6,10,15,19,23-hexamethyltetracosane, $C_{30}H_{62}$) was chosen due to its suitable physical properties of low melting temperature (−38 °C) and low vapor pressure ($\sim 2 \times 10^{-8}$ Torr) at room temperature. A continually refreshed liquid surface is produced using a rotating stainless steel wheel immersed in a copper bath filled with squalane and a Teflon spacer. The temperature of the bath is controlled using a Peltier element. It was maintained at a fixed value typically between −10 °C and +80 °C. Independent tests showed that these correspond to liquid squalane temperatures on the wheel under vacuum of (0 ± 1) °C and (70 ± 1) °C, respectively.

The liquid surface apparatus is contained within a six-armed stainless steel reaction chamber. The 355 nm third harmonic of a Nd:YAG laser (Continuum Surelite SLII-10) with a typical energy of 120 mJ in a ~5 ns pulse passes through the chamber at a selected distance, typically in the range 4−15 mm, above the liquid surface. This produces $O(^3P)$ atoms by photolysis of NO_2 (BOC, 98.3%) gas, which is admitted into the chamber at a typical pressure of 1 mTorr. The laser polarization was selected to optimize the fraction of the moderately anisotropic angular distribution of $O(^3P)$ atoms recoiling toward the surface.[13] The oxygen atom speed distribution is relatively broad, with an average collision energy of 15.8 kJ mol^{-1} and a full width at half maximum of around 26 kJ mol^{-1}.[12b]

A fraction of the $O(^3P)$ atoms react by abstracting a hydrogen atom from the liquid surface to form OH radicals. These hydroxyl radicals are then detected by LIF on the well-known A−X band using a counter-propagating Nd:YAG (Spectron Laser Systems SL803S) pumped tunable dye laser (Spectron Laser Systems SL4000G) with a typical pulse energy of 1 mJ. Fluorescence was collected perpendicular to the laser beams and passed through a liquid light guide (Ultrafine Technology Ltd.) positioned approximately 1 cm above the laser axis. Fluorescence on selected emission bands was isolated using custom interference filters before being detected by a photomultiplier tube (PMT, Electron Tubes Ltd.).

The signal from the PMT was captured by a transient digitizer incorporated in a CAMAC modular data acquisition system interfaced to a PC. All processing and data analysis was carried out by a PC using a custom-written LabVIEW program. The software was also used to control, via appropriate modules, experimental parameters such as the relative timings of the laser systems and the wavelength of the dye laser.

Results

As we have established previously,[12b] it is possible to simulate the time-of-flight profiles by assuming that two different components contribute to the overall distribution: a thermal,

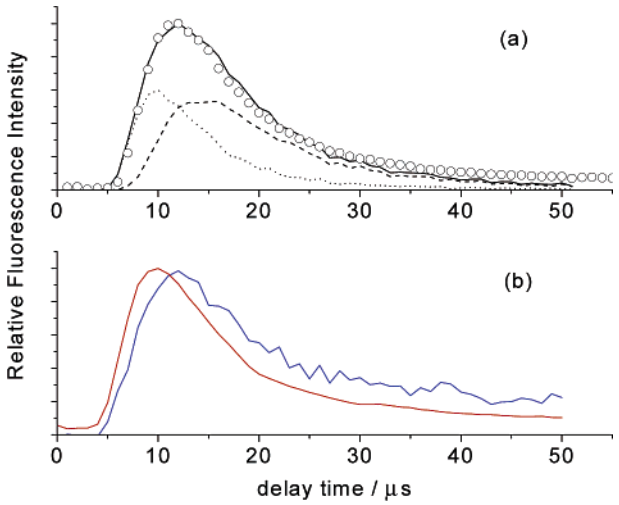

Figure 1. (a) Measured and simulated profiles of OH ($v' = 0$) after reaction of O(^{3}P) atoms with a liquid squalane surface. Open circles are experimental data. Dotted and dashed lines are the direct and thermal components of the Monte Carlo simulation,[12b] respectively, and the solid line is a combination of both. Liquid temperature = 298 K; $p(NO_2)$ = 1 mTorr; distance surface−probe laser = 4.5 mm. (b) Measured appearance profiles of OH after reaction of O(^{3}P) atoms with a liquid squalane surface. Profiles were recorded on the $Q_1(1)$ line of the (1,0) and (2,1) bands, shown as red and blue lines, respectively. Liquid surface temperature = 298 K; $p(NO_2)$ = 2 mTorr; distance surface−probe laser = 6 mm.

trapping-desorption mechanism and a direct, dynamical abstraction, in a ratio of around 60:40. Crucially, the sharp onset of the measured appearance profiles *cannot* be simulated successfully without the contribution from the higher-velocity direct component, as reproduced in Figure 1a. Thermally accommodated OH radicals are simply not moving fast enough to account for the measured profiles at the earliest times. This enables the important extension we report here in which the internal state distribution of the faster, presumed to be direct, component is isolated by exploiting its shorter time-of-flight. Importantly, separate appearance profiles for OH ($v' = 0$) and ($v' = 1$) were measured accurately for the first time and are reported in Figure 1b. Each measurement was made under the same conditions of NO_2 pressure and liquid surface temperature, and with great care being taken to ensure that the laser-surface distance was the same in both cases. It is clear from these profiles that the OH radicals in ($v' = 0$) start to rise and peak earlier than those in ($v' = 1$). The point at which to measure nascent rotational state distributions of the faster component was therefore selected appropriately for each vibrational level. For a laser beam-to-surface distance of 5 mm, the time delay between the photolysis and the probe laser was set to 6 μs for ($v' = 0$) and 8 μs for ($v' = 1$). According to the Monte Carlo simulations, this should result in a contribution from the direct component of ≥90% in both cases.

We note that it is not currently possible for us to achieve the complementary isolation of the trapping−desorption component. This is partially because of the breadth of the O(^{3}P) velocity distribution produced in the NO_2 photolysis. It is also because collision-free conditions are not maintained at the longer times required to observe low-velocity products at practical precursor pressures. As we have noted previously,[12] we believe the onset of the secondary collisions is responsible for the increasing discrepancy between predicted and observed profiles at longer times in Figure 1a.

LIF excitation spectra were obtained at the rising edge of the appearance profiles over wavelength ranges that covered

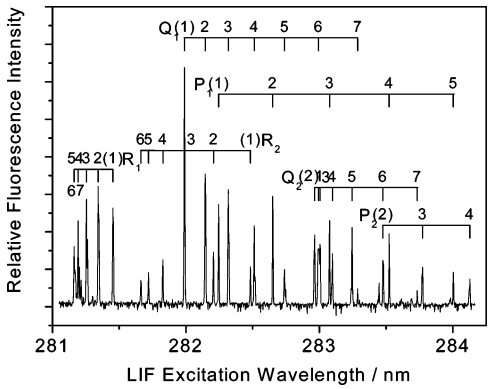

Figure 2. Representative OH A−X (1,0) LIF excitation spectrum recorded at the rising edge after reaction of O(^{3}P) atoms with a liquid squalane surface. Liquid temperature = 343 K; $p(NO_2)$ = 1 mTorr; distance surface−probe laser ∼ 5 mm; photolysis−probe delay = 6 μs.

both F_1 and F_2 fine-structure manifolds of both OH vibrational levels. The measurements were repeated at two distinct liquid surface temperatures, (273 ± 1) K and (343 ± 1) K. Figure 2 shows a typical rising-edge spectrum, illustrating the very satisfactory signal-to-noise ratio achievable under "nascent" conditions.

Rotational population distributions were derived from the nascent spectra by calibration against a thermal OH spectrum, as we have described previously.[12] These thermal spectra were recorded under conditions in which the hydroxyl radicals undergo ∼15 collisions on average with added background gas, N_2. We believe that this is sufficient for the OH radicals to thermally equilibrate from a rotational distribution that does not in practice deviate much from a thermal distribution in the first place. The nascent rotational distributions were then determined from the ratio of signals in the nascent and thermal spectra, using straightforward Boltzmann statistics to calculate the thermal populations.

Figure 3 shows representative Boltzmann plots of the F_1 manifold for both OH ($v' = 0$) and ($v' = 1$) at liquid surface temperatures of 273 and 343 K.

Measurements at the rising edge (top panel) are compared to previous measurements at the peak of the appearance profiles. The plots demonstrate two key observations. The rotational distributions at the rising edge are not influenced by the liquid surface temperature to the same degree as those at the peak, particularly for ($v' = 0$). Also in contrast with the peak, the rotational distributions of ($v' = 0$) and ($v' = 1$) differ from each other significantly more at the rising edge. Since these plots are in all cases approximately linear, it is convenient for the purposes of comparison to summarize each distribution by a single nominal rotational temperature. These temperatures are summarized in Table 1, allowing the key points just identified to be made more quantitatively. For this purpose, the F_1 and F_2 manifolds have been averaged appropriately. It can be seen that rotational temperatures in ($v' = 1$) are always colder than those in ($v' = 0$), but this effect is far more pronounced when measured at the rising edge (on average 111 K) than at the peak (45 K). It is also obvious that the liquid surface temperature has a clear impact on the rotational temperature, but only when measured at the peak. The rotational temperatures at the peak increase by 26 K for ($v' = 0$) and 39 K for ($v' = 1$) when the surface temperature is raised by 70 K. The differences are distinctly smaller at the rising edge, where the rotational temperature increases by only 14 K for ($v' = 1$) while it

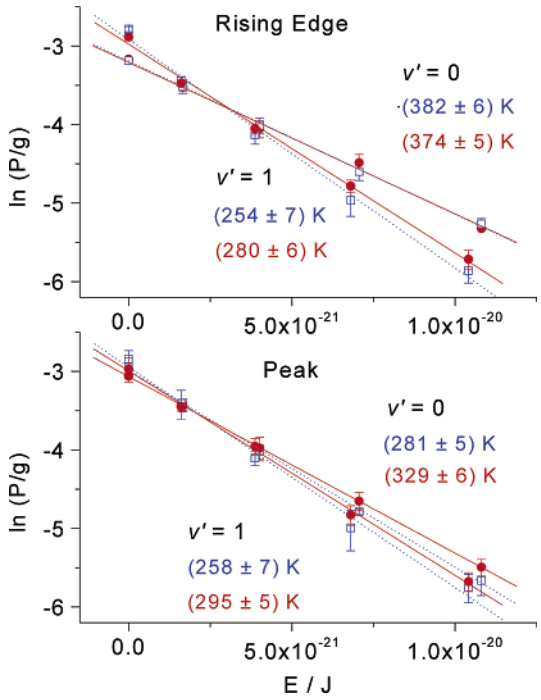

Figure 3. Boltzmann plots (natural log of relative population, P, divided by rotational degeneracy, g, against rotational energy, E) of the rotational distributions in the F_1 manifold of OH ($v' = 0$) and ($v' = 1$). Upper panel: rising edge (photolysis−probe delay of 6 or 8 μs for ($v' = 0$) and ($v' = 1$), respectively). Lower panel: peak (typical photolysis−probe delay of 10 μs). Liquid surface temperatures of 273 K (blue squares) and 343 K (red circles). $p(NO_2) = 1$ mTorr; distance surface−probe laser ~ 5 mm.

TABLE 1: Rotational Temperatures of Nascent OH ($v' = 0$) and ($v' = 1$) Averaged over F_1 and F_2 Manifolds[a]

	rising edge		peak	
surface temp/K	273	343	273	343
($v' = 0$)	381 ± 5	373 ± 5	304 ± 3	330 ± 5
($v' = 1$)	259 ± 6	273 ± 5	253 ± 5	292 ± 4

[a] Liquid temperatures of either 273 or 343 K, as indicated; photolysis-probe delay 6 or 8 μs for ($v' = 0$) and ($v' = 1$), respectively, at the rising edge and ~10 μs at the peak; $p(NO_2) = 1$ mTorr; distance surface−probe laser ~ 5 mm.

nominally decreases by 8 K for ($v' = 0$). Such small differences are approaching the limit where they may not be statistically significant.

We also note that in most cases the rotational temperatures converge as expected toward the liquid surface temperature, but from opposite directions, when going from the rising edge to the peak. The exception is the apparent slight decrease of the rotational temperature in ($v' = 1$) at a liquid surface temperature of 273 K. However, this may also not be statistically significant because of the small difference (of only 14 K) between the nascent OH rotational temperature and the surface temperature.

Discussion

The key aspect of the results that we seek to explain is the relationship of the observed OH rovibrational distributions at the rising edge of the time-of-flight profiles to those measured previously at the peak. In summary, we had established previously[12b] that the rotational temperature at the peak is correlated with the liquid surface temperature, but, importantly, only partially. This suggests that some, but not all, of the OH is accommodated at the liquid surface before escaping. On the other hand, the rotational temperatures in ($v' = 1$) remain moderately colder than those in ($v' = 0$). This is reminiscent of the larger difference expected from a direct mechanism (see below). We concluded from these combined observations that two different components contribute to the overall distribution, namely a thermal, trapping−desorption component and a direct abstraction. Our discussion here is focused mainly on the extent to which the new results reinforce the correct mechanistic assignment of the direct component by observing it in isolation.

Beginning with the OH rotational temperatures in Table 1, the new results at the rising edge of the time-of-flight profiles do *not*, in contrast, show a strong correlation with the liquid surface temperature, for either ($v' = 0$) and ($v' = 1$). The main inference from these results is that the hydroxyl radicals at the rising edge have little "memory" of the surface temperature. This is directly at odds with a trapping−desorption mechanism and strongly enhances the conclusion that they result from a direct abstraction mechanism. A direct process might reasonably be expected to couple relatively little of the surface thermal energy into product rotational motion. This is not to say that there is intrinsically no possible effect of the surface temperature on product rotation in a direct mechanism. Such an effect could result, for example, from dynamical coupling of thermal energy in vibrational or hindered rotational modes of the liquid surface into OH product rotation. When averaged over ($v' = 0$) and ($v' = 1$), our rising-edge data do actually suggest a slight net increase in OH rotational temperature on going between surface temperatures of 273 and 343 K. Care should be exercised not to over-interpret such subtle secondary effects, though, because their statistical significance is very marginal. There could easily be other, simpler explanations, such as small residual underlying contributions from the thermal component at early times, perhaps to varying degrees for ($v' = 0$) and ($v' = 1$).

Perhaps yet more striking, the second piece of evidence supporting the main conclusion is the difference between the rotational temperatures for ($v' = 1$) and ($v' = 0$). These amount to 122 and 100 K for liquid surface temperatures of 273 and 343 K, compared to only 51 and 38 K at the peak for the same surface temperatures (see Table 1). The larger differences are strongly characteristic of a direct process, where the constraint on total energy imposes lower rotational energies on the higher vibrational levels. It is instructive to compare them with typical OH rotational temperatures from the related reactions between $O(^3P)$ atoms and gas-phase hydrocarbons.[14] The largest hydrocarbon that has been investigated extensively, cyclohexane C_6H_{12}, yields rotational temperatures of (376 ± 18) K for OH ($v' = 0$) and (197 ± 18) K for ($v' = 1$).[15] These are similar at a qualitative level to those of the direct component here. Any more quantitative agreement would not necessarily be expected for a number of reasons. The nature of the hydrogen atoms is known to have a small effect on the OH rotational temperature.[14] Only secondary hydrogen atoms can be abstracted from C_6H_{12}, whereas a combination of primary, secondary, and tertiary hydrogen atoms is available for squalane. There is also a known small effect of the collision energy on the rotational distributions in the gas-phase and the center-of-mass energies employed in gas-phase experiments do not necessarily match those in the present work.

Nevertheless, the qualitatively similar rotational distributions in the gas-phase and gas−liquid interfacial reaction strongly suggest that the mechanism of the direct component is very similar to the gas-phase reaction. This is well-established, through a wide range of independent experimental evidence and corroborating theoretical predictions, to be a direct abstraction

via a transition state with a C−H−O angle near 180°. We therefore strongly reinforce our conclusion that the direct component must originate from O(^{3}P) reaction through a near-collinear interaction with a H−C unit in a part of the hydrocarbon chain that is exposed at the outer surface of the liquid, followed by direct OH recoil into the gas-phase without any secondary encounters.

As a secondary point, we note from Table 1 that the rotational temperature in OH ($v' = 1$) does not generally appear to 'warm up' as much as ($v' = 0$) 'cools down' when going from the rising edge to the peak. This may simply be attributed to the finite experimental precision combined with the fact that the difference between the nascent rotational distribution of the direct component and the target temperature of the liquid surface tends to be accidentally greater for ($v' = 0$) than for ($v' = 1$). However, it is also possible that the ratio between trapping−desorption and direct mechanisms is lower for ($v' = 1$) than for ($v' = 0$). This is plausible, as trapped OH ($v' = 1$) may be vibrationally relaxed at the surface, a channel obviously absent for ($v' = 0$). Secondary reaction with the hydrocarbon to produce H_2O may also be enhanced by OH vibrational relaxation. Both these pathways may contribute to an apparent overall loss of the trapping−desorption mechanism in ($v' = 1$), while the direct mechanism would not be affected. This would tend to influence the ratio in favor of the direct mechanism, consistent with our current results.

The third main strand of evidence in favor of the assignment to a direct mechanism at early times is the distinct time-of-flight profiles in Figure 1b. These clearly demonstrate that the external translational energy of the ($v' = 1$) component is lower than for ($v' = 0$). Consistent with its production via a direct mechanism, the extra internal energy needed to populate the higher vibrational level is not available for translation, producing slower and, as already noted above, rotationally less excited, OH ($v' = 1$). The profiles link our work, designed primarily to measure accurate internal energy distributions, and that of Minton and co-workers who measured much more highly resolved energy (and angular) distributions by time-of-flight mass spectrometry.[8,11] Naturally, though, mass spectrometric detection does not distinguish between internal states. What we have been able to show unequivocally for the first time here is that there is a correlation between the kinetic energy of the early-time component and the corresponding internal energy.

It is not straightforward, however, to analyze more quantitatively the energy released to different degrees of freedom as a fraction of the total energy available. As we have noted above and discussed previously,[12b] the distribution of collision energies in our experiments is relatively broad. The exothermicity of reaction is similarly ill-defined because of the unknown relative contributions from primary, secondary and tertiary C−H sites. In isolated hydrocarbon molecules, the exothermicity of the abstraction reaction varies in this sequence from around −5 to −25 kJ mol^{-1} (although even the basic thermochemistry is open to a perhaps surprising level of uncertainty[14]). Furthermore, it is an open question as to whether this is substantially affected by intermolecular reorganizational energies on production of the hydrocarbon radical in the condensed phase, which may be a possible explanation for the empirical observation of enhanced reactivity relative to the analogous gas-phase reactions.[7]

Speculating somewhat more widely, we believe that the very close similarity of the product state distributions to those for isolated hydrocarbons in the gas phase also implies that the direct component, at least, of the gas−liquid reaction is confined to the triplet electronic surface. An insertion mechanism involving crossing to a singlet electronic surface has been suggested previously by Naaman[7b] as a possible explanation for the enhanced reactivity of O(^{3}P) at condensed-phase hydrocarbon surfaces observed in related kinetic measurements.[7] Any OH produced by this route would almost certainly have a distinct product state distribution. We interpret our data to suggest that the direct mechanism makes a contribution of around 40% to the total yield of OH, estimated previously from the fit to time-of-flight profiles.[12b] In other words, only around half of the total OH yield is produced via all possible mechanisms other than direct abstraction. Our data do not therefore appear to support the idea that an electronic surface-hopping is responsible for substantially enhanced reactivity at the liquid surface, at least on this OH-producing channel.

Finally, our experimental results can be compared briefly with the most closely related theoretical work currently available.[16] As yet, no dynamical simulations of the reaction of O(^{3}P) with hydrocarbon liquids have been published, but Hase and co-workers and Schatz and co-workers have independently simulated the reaction with self-assembled monolayers (SAMs) composed of alkyl chains. Both groups modeled SAMs of six to eight carbon atoms and performed "on-the-fly" quasi-classical trajectory calculations of their reaction with O(^{3}P). The potentials controlling the motions of the underlying gold layer, the sulfur atoms, and the lower hydrocarbon segments were generated by (classical) molecular mechanics, whereas those for the outer hydrocarbon groups and the incoming oxygen atoms were treated quantum-mechanically. The main difference between the two sets of calculations is that the earlier work by Hase and co-workers considered lower incident O(^{3}P) energies of 1.2, 5.0, 11.2, and 19.1 kcal mol^{-1}, whereas the work by Troya and Schatz assumed hyperthermal O(^{3}P) atoms with kinetic energies of 5 eV (115 kcal mol^{-1}), having been motivated by the LEO problem mentioned above.

Both theoretical studies found very little OH vibrational excitation. This is therefore in good accord with our experiments.[12] Hase and co-workers assigned a low but slightly higher than thermal energy to OH rotation. Troya and Schatz analyzed the rotational energy in the direct and the trapping−desorption component separately, finding the trapping−desorption component to be cold with a hotter distribution in the direct mechanism. Our own experimental results make a further distinction, not reported in the calculations, between the rotational excitation in ($v' = 1$) and ($v' = 0$). Nevertheless, for ($v' = 0$), our slightly hotter than thermal rotational temperature in the direct component is successfully qualitatively reproduced, although quantitatively over-estimated, by the theoretical work.

Troya and Schatz argue that the low rotational excitation of the trapping−desorption component is due to hindered rotation when the OH is trapped within the hydrocarbon chain. While this specific "dynamical" explanation might indeed be a feature of the more-structured model SAMs and perhaps also of real liquids, it is not possible from the results of our current experiments to distinguish it from the simpler, essentially statistical assumption that the trapped OH adopts the temperature of the liquid.

Conclusion

We have investigated successfully the benchmark interfacial reaction between O(^{3}P) atoms and liquid squalane, $C_{30}H_{62}$, by combining time-of-flight resolution with state-selective spectroscopic detection. The new results strengthen considerably the previous conclusion that the mechanism consists of two channels: a faster, direct component, with nonequilibrium internal

energy distributions characterized here for the first time, is accompanied by a slower, rotationally equilibrated trapping−desorption component. Several new strands of evidence combine to support these mechanistic conclusions. The fastest OH ($v' = 0$) has a higher translational energy than ($v' = 1$), consistent with the total energy constraint expected for a direct mechanism. Also consistent with this constraint is the large difference between ($v' = 0$) and ($v' = 1$) rotational temperatures at the rising edge. The weak dependence on the bulk liquid temperature further suggests a direct mechanism in which there is little coupling of the surface thermal motion into OH product rotation. On the basis of the close correspondence of measured rotational distributions, it is very likely that this is a near-collinear, direct abstraction mechanism of the type previously established for the corresponding homogeneous gas-phase reaction. The difference between ($v' = 0$) and ($v' = 1$) rotational temperatures diminishes, while the dependence on bulk temperature increases, at the peak of the profile. This is consistent with an increased contribution from a trapping−desorption component in which rotational and translational (but not vibrational) motions have been thermally accommodated.

Acknowledgment. We thank the Engineering and Physical Sciences Research Council for a research grant and M.A.'s scholarship. M.L.C. thanks the Royal Society of Edinburgh and Research Councils UK for fellowships. S.P.K.K. thanks the Fonds der Chemischen Industrie for a scholarship. The authors also thank David A. Henderson and Hailey Kelso for development of the apparatus and Ian Drummond for technical input.

References and Notes

(1) (a) Whitehead, J. C. *Rep. Prog. Phys.* **1996**, *59*, 993−1040. (b) Simons, J. P. *Faraday Discuss.* **1999**, *113*, 1−25. (c) Casavecchia, P.; Balucani, N.; Volpi, G. G. *Annu. Rev. Phys. Chem.* **1999**, *50*, 347−376. (d) Valentini, J. J. *Annu. Rev. Phys. Chem.* **2001**, *52*, 15−39. (e) Liu, K. *Annu. Rev. Phys. Chem.* **2001**, *52*, 139−164.

(2) (a) Langmuir, I. *Trans. Faraday Soc.* **1922**, *17*, 621−675. (b) Rettner, C. T.; Auerbach, D. J. *Science* **1994**, *263*, 365−367.

(3) Hurlbut, F. C.; Beck, D. E. U. C. Eng. Proj. Report HE-150-166; University of California, 1959.

(4) (a) Saecker, M. E.; Govoni, S. T.; Kowalski, D. V.; King, M. E.; Nathanson, G. M. *Science* **1991**, *252*, 1421−1424. (b) Saecker, M. E.; Nathanson, G. M. *J. Chem. Phys.* **1993**, *99*, 7056−7075.

(5) (a) Kenyon, A. J.; McCaffery, A. J.; Quintella, C. M.; Zidan, M. D. *Chem. Phys. Lett.* **1992**, *190*, 55−58. (b) Perkins, B. G., Jr.; Haber, T.; Nesbitt, D. J. *J. Phys. Chem. B.* **2005**, *109*, 16396−16405.

(6) (a) Blanchard, D. C. *Science* **1964**, *146*, 396−397. (b) Vaida, V.; Tuck, A. F.; Ellison, G. B. *Phys. Chem. Earth (C)* **2000**, *25*, 195−198.

(7) (a) Moise, T.; Rudich, Y. *Geophys. Res Lett.* **2001**, *28*, 4083−4086. (b) Paz, Y.; Trakhtenberg, S.; Naaman, R. *J. Phys. Chem.* **1994**, *98*, 13517−13523. (c) Bertram, A. K.; Ivanov, A. V.; Hunter, M.; Molina, L. T.; Molina, M. J. *J. Phys. Chem. A* **2001**, *105*, 9415−9421.

(8) Zhang, J.; Garton, D. J.; Minton, T. K. *J. Chem. Phys.* **2002**, *117*, 6239−6251.

(9) Qin, X.; Tzvetkov, T.; Liu, X.; Lee, D.-C.; Yu, L.; Jacobs, D. C. *J. Am. Chem. Soc.* **2004**, *126*, 13232−13233.

(10) Murr, L. E.; Kinard, W. H. *Am. Sci.* **1993**, *81*, 152−165.

(11) (a) Garton, D. J.; Minton, T. K.; Alagia, M.; Balucani, N.; Casavecchia, P.; Volpi, G. G. *Faraday Discuss. Chem. Soc.* **1997**, *108*, 387−399. (b) Garton, D. J.; Minton, T. K.; Alagia, M.; Balucani, N.; Casavecchia, P.; Volpi, G. G. *J. Chem. Phys.* **2000**, *112*, 5975−5984. (c) Garton, D. J.; Minton, T. K.; Alagia, M.; Balucani, N.; Casavecchia, P.; Volpi, G. G. *J. Chem. Phys.* **2001**, *114*, 5958.

(12) (a) Kelso, H.; Köhler, S. P. K.; Henderson, D. A.; McKendrick, K. G. *J. Chem. Phys.* **2003**, *119*, 9985−9988. (b) Köhler, S. P. K.; Allan, M.; Kelso, H.; Henderson, D. A.; McKendrick, K. G. *J. Chem. Phys.* **2005**, *122*, 024712.

(13) Baker, R. P.; Costen, M. L.; Hancock, G.; Ritchie, G. A. D.; Summerfield, D. *Phys. Chem. Chem. Phys.* **2000**, *2*, 661−664.

(14) Ausfelder, F.; McKendrick, K. G. *Prog. React. Kinet.* **2000**, *25*, 299−370.

(15) Ausfelder, F.; Kelso, H.; McKendrick, K. G. *Phys. Chem. Chem. Phys.* **2002**, *4*, 473−481.

(16) (a) Li, G.; Bosio, S. B. M.; Hase, W. L. *J. Mol. Struct.* **2000**, *556*, 43−57. (b) Troya, D.; Schatz, G. C. *J. Chem. Phys.* **2004**, *120*, 7696−7707.